

# Reactive Power Injection Strategies for Single-Phase Photovoltaic Systems Considering Grid Requirements

Yongheng Yang, *Member, IEEE*, Huai Wang, *Member, IEEE*, and Frede Blaabjerg, *Fellow, IEEE*

**Abstract**—As the development and installation of photovoltaic (PV) systems are still growing at an exceptionally rapid pace, relevant grid integration policies are going to change consequently in order to accept more PV systems in the grid. The next-generation PV systems will play an even more active role like what the conventional power plants do today in the grid regulation participation. Requirements of ancillary services like low-voltage ride-through (LVRT) associated with reactive current injection and voltage support through reactive power control have been in effectiveness in some countries, e.g., Germany and Italy. Those advanced features can be provided by next-generation PV systems and will be enhanced in the future to ensure an even efficient and reliable utilization of PV systems. In light of this, reactive power injection (RPI) strategies for single-phase PV systems are explored in this paper. The RPI possibilities are as follows: 1) constant average active power control; 2) constant active current control; 3) constant peak current control; and 4) thermal optimized control strategy. All those strategies comply with the currently active grid codes but are with different objectives. The proposed RPI strategies are demonstrated first by simulations and also tested experimentally on a 1-kW single-phase grid-connected system in LVRT operation mode. Those results show the effectiveness and feasibilities of the proposed strategies with reactive power control during LVRT operation. The design and implementation considerations for the characterized RPI strategies are also discussed.

**Index Terms**—Grid requirements, junction temperature, low-voltage ride-through (LVRT), photovoltaic (PV) systems, power (PQ) control, reactive power injection, reliability, single-phase systems.

## I. INTRODUCTION

THE advancements of power electronics technologies have shown great potential for renewable energy integration into the grid, as proved by the continuously booming penetration level of photovoltaic (PV) systems [1]–[5], which leads to increased grid decentralization and vulnerability. Hence, catering for further more PV installations calls for advanced control strategies in compliance with grid requirements or standards.

Manuscript received December 2, 2013; revised March 12, 2014 and June 14, 2014; accepted June 16, 2014. Date of publication August 8, 2014; date of current version November 18, 2014. Paper 2013-IPCC-0972.R2, presented at the 2014 IEEE Applied Power Electronics Conference and Exposition, Fort Worth, TX, USA, March 16–20, and approved for publication in the IEEE TRANSACTIONS ON INDUSTRY APPLICATIONS by the Industrial Power Converter Committee of the IEEE Industry Applications Society.

The authors are with the Department of Energy Technology, Aalborg University, 9220 Aalborg, Denmark (e-mail: yoy@et.aau.dk; hwa@et.aau.dk; fbl@et.aau.dk).

Color versions of one or more of the figures in this paper are available online at <http://ieeexplore.ieee.org>.

Digital Object Identifier 10.1109/TIA.2014.2346692

Currently, it is required that the PV systems cease to energize local loads in the presence of grid abnormal conditions, e.g., voltage sags and frequency variations [6]–[11]. Meanwhile, it is required in those grid regulations for most systems to operate at unity power factor (or a minimum power factor, e.g., power factor  $\geq 0.9$ ) with maximum power point tracking (MPPT) control in order to extract as much energy as possible from the PV panels [11]–[14]. Those grid requirements are valid in case of a low penetration degree of PV systems, including the most commonly used single-phase systems.

However, a still increasing adoption of PV systems will violate the grid integration. For example, potential overloading or voltage rises may appear at distributed grid feeders, particularly when a very high penetration level of PV systems is reached, due to the intermittent nature of solar PV source and the unbalance between PV supply and load demands [2], [4], [10], [15]–[21]. Possibilities to solve those issues include limiting feed-in maximum power from PV systems [22] and reducing installations, which are against the goal of carbon reduction in most countries, e.g., Germany, by enabling an even more wide-scale adoption of renewable energies. Thus, those countries have put forward specific grid requirements for large-scale PV systems, which should be able to participate in voltage regulation through reactive power control (injecting or absorbing reactive power), as static grid support [23]–[26].

Meanwhile, the trip-off of an aggregated PV system owing to anti-islanding protection may induce grid variations, leading to more serious events, e.g., power outage [4], [10], [21], [27]–[29]. Hence, in response to grid disturbances, it is better for next-generation PV systems to provide dynamic grid support in terms of low-voltage ride-through (LVRT) with reactive power injection (RPI), in order to do the following: 1) stabilize the grid in case of failures and 2) avoid loss of massive PV generation systems. For instance, in Italy, any generation system with the total power exceeding 6 kW should have LVRT capability [24]. In Germany, it has been in effectiveness for medium- or high-voltage systems, including grid-connected PV systems [4], [28]–[32]. Other countries also keep the pace with grid code revisions [10], [33]–[35]. Those requirements were first introduced to wind turbine systems but, today, tend to be extended to all PV systems, even for PV modules [34]. Obviously, the implementation of LVRT function violates the anti-islanding requirement. Hence, as shown in Fig. 1, the compatibility of those two functions should be taken into consideration when upgrading grid requirements.

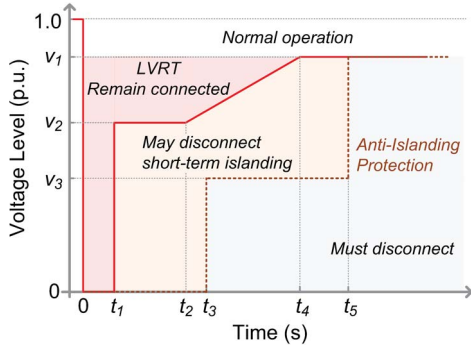


Fig. 1. Suggestion on a compatible implementation of low-voltage (and zero-voltage) ride-through and anti-islanding requirements for single-phase PV systems connected to low-voltage networks.

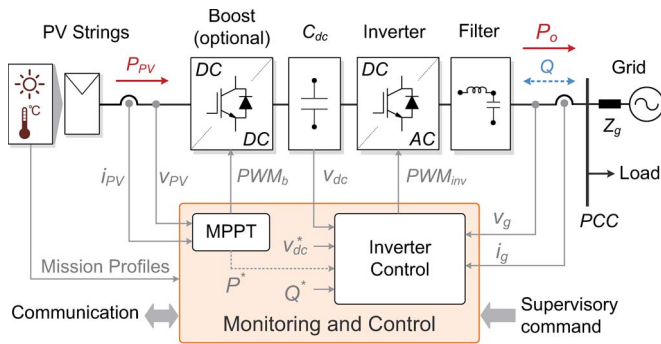


Fig. 2. Typical power and control configuration of a single-phase grid-connected PV system.

Nonetheless, as the penetration level is continuously growing, much controllability of active power and reactive power should be ensured in future PV systems, including reactive power control to support the grid voltage statically (voltage rise mitigation) and also ride-through faults dynamically, which is associated with RPI control during the transients. In light of the aforementioned issues, this paper explores single-phase RPI strategies, including the following: 1) constant average active power control; 2) constant active current control; 3) constant peak current control; and 4) thermal optimized reactive power control strategy. First, a brief introduction of the power control for single-phase PV systems is given in Section II, followed by the proposed RPI methods. Simulations and experiments were carried out on a 1-kW single-phase system in the LVRT operation mode and presented in Section IV. Both results have verified the effectiveness of the proposed RPI strategies.

II. POWER CONTROL OF SINGLE-PHASE SYSTEMS

Since the PV systems are still dominantly for residential applications at present, single-phase topologies are more widely used solutions for PV systems. Fig. 2 represents a typical single-phase grid-connected PV system, where, in some cases, a dc–dc converter is adopted to boost up the PV panel voltage within an acceptable range of the PV inverter [6], [9], [11]. It also offers the flexibility of MPPT control, which is a basic requirement for such systems operating at unity power factor. Meanwhile, the injected current should be synchronized with

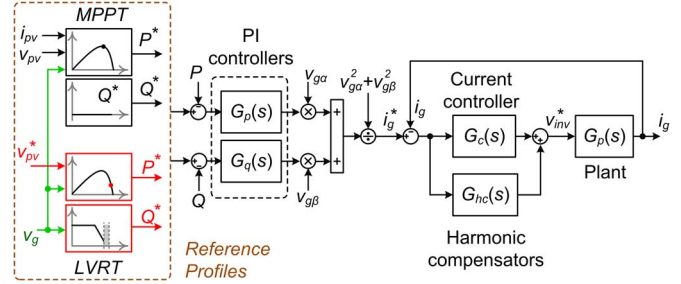


Fig. 3. Control structure in the  $\alpha\beta$ -frame for single-phase single-stage PV systems based on single-phase  $PQ$  theory [11], [40].

the grid voltage, and as mentioned previously, the system should disconnect from the grid when it presents disturbances (e.g., frequency or voltage variation) at the point of common coupling (PCC), as shown in Fig. 2.

As for the control of single-phase systems with the RPI function, the droop control concept [8], [36] for single-phase PV systems is not suitable since it requires that the line is mainly inductive (i.e.,  $X \gg R$ ). The utilization of adaptive filtering technique leads to an instantaneous power control solution [37]. This power control method is a good candidate for single-phase systems when a satisfactory synthesis of the power references is achieved. Aside from the aforementioned possibilities, the power control can also be developed in the  $dq$ - or  $\alpha\beta$ -frame, based on the single-phase  $PQ$  theory [11], [37]–[42]. The implementation of this control solution is intuitive with less complexity, but it requires an orthogonal-signal-generation system to create quadrature components ( $v_{g\alpha}$ ,  $v_{g\beta}$  and  $i_{g\alpha}$ ,  $i_{g\beta}$ ) corresponding to the real grid voltage  $v_g$  and current  $i_g$ , as shown in Fig. 3. Moreover, a power calculation method in terms of fast computation and high accuracy can contribute to the control performance.

Thus, the RPI control can be implemented in this control solution as the “Reference Profiles” by setting the references for active power  $P^*$  and reactive power  $Q^*$ , and then, the grid current reference  $i_g^*$  is generated. In normal operation mode, the active power reference  $P^*$  is the tracked maximum power  $P_{MPP}$  of the PV panels ( $P^* = P_{MPP}$ ), and  $Q^* = 0$  var. When the RPI control is enabled by a detected grid condition (voltage and frequency range), the reactive power is injected according to the grid requirements, e.g., the German grid code shown in Fig. 4(a) [4], [29]. It is noted that, during fault ride-through operation, the system should inject sufficient reactive current according to the grid voltage level [4], [29], [31]. This relationship can be defined as

$$k = \frac{(I_q - I_{q0})/I_N}{(1 - v_g)}, \text{ when } I_q < I_N \quad (1)$$

where  $I_{q0}$  is the initial reactive current before grid failure and  $v_g$  is the instantaneous voltage in per unit (p.u.) during voltage fault. Since the PV systems are required to operate at unity power factor in MPPT mode, there is no reactive power injection before voltage sags, i.e.,  $I_{q0} = 0$  A. Moreover, it is required by this grid code that  $k$  should be larger than 2 p.u., i.e.,  $k \geq 2$  p.u., for a minimum reactive current injection [29].

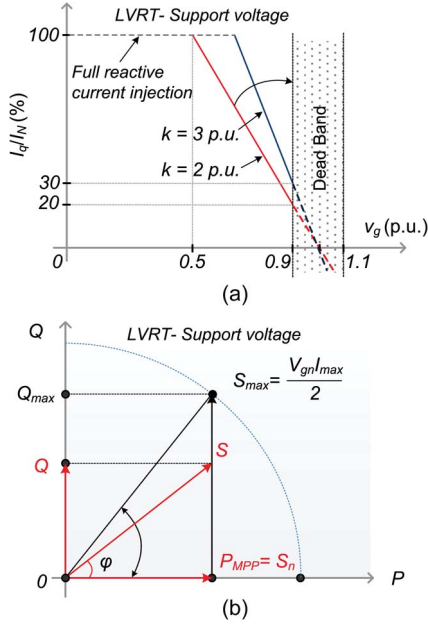


Fig. 4. Reactive power profiles for single-phase systems: (a) During LVRT for medium- and/or high-voltage systems [29], [31], [43] and (b) reactive power capability of a PV inverter.

For example, when the grid voltage sags to 0.8 p.u., a minimum reactive current  $I_q$  (40% of the rated current  $I_N$ ) should be injected into the grid. It is also shown in Fig. 4(a) that, under a severe voltage fault (e.g.,  $v_g = 0.3$  p.u.), full reactive power injection should be enabled, where the active power injection could be deactivated. However, the amount of reactive power is limited by the inverter apparent power  $S_{\max}$ , as illustrated in Fig. 4(b). This constraint should be taken into account when designing the RPI strategies, i.e., the avoidance of inverter trip-off due to overcurrent protection.

### III. REACTIVE POWER INJECTION STRATEGIES

Some grid specifications have been imposed on the next-generation PV systems, particularly for medium-/high-voltage applications [26], [27]. In the future, PV systems, covering a wide range of applications, have to provide reactive power under grid faults. As discussed in the last paragraph, when designing the RPI control strategies, both the grid requirements [e.g., Fig. 4(a)] and the inverter current limitation shown in Fig. 4(b) have to be complied. Those constraints are given as

$$\begin{cases} I_q = I_N, & 0 \leq v_g < (1 - \frac{1}{k}) \text{ p.u.} \\ I_q = k(1 - v_g)I_N, & (1 - \frac{1}{k}) \text{ p.u.} \leq v_g < 0.9 \text{ p.u.} \end{cases} \quad (2)$$

where  $k \geq 2$  p.u. is defined in (1) and

$$I_{g \max} = \sqrt{I_d^2 + I_q^2} \leq I_{\max} \quad (3)$$

in which  $I_d$  is the active current,  $I_{g \max}$  is the amplitude of the injected current, and  $I_{\max}$  is the inverter allowable maximum current level. In accordance with (2) and (3), the following RPI strategies are proposed.

#### A. Constant Average Active Power Control (Const.-P)

The objective of this RPI control strategy is to maximize the output energy with MPPT control during LVRT operation. Therefore, the average active power is maintained constant in the short-term period. Based on the single-phase  $PQ$  theory, the average active power can be given as

$$P = \frac{1}{2} v_{gm} I_d \quad (4)$$

where  $v_{gm}$  is the amplitude of the grid voltage during MPPT operation and  $I_d$  is the active current of the injected grid current. In the normal operation mode,  $I_d = I_N$ , and hence, under LVRT situation with *Const.-P* control, the average active power  $P = k_d P_N = (k_d/2) v_{gmn} I_N$ , with  $v_{gmn}$  and  $I_N$  being the nominal values of the grid voltage and current, respectively, and  $k_d$  being the power derating factor.

According to (2) and (4), when the instantaneous grid voltage level  $v_g$ :  $(1 - (1/k))$  p.u.  $\leq v_g < 0.9$  p.u., the current in the  $dq$ -frame can be expressed as

$$\begin{cases} I_d = \frac{k_d}{v_g} I_N \\ I_q = k(1 - v_g) I_N \end{cases} \quad (5)$$

in which  $k$  is defined in (1) and  $k_d$  has been given previously. When the grid voltage level sags to lower than  $(1 - (1/k))$  p.u. (i.e., a severe voltage sag occurs), the system is required to fully inject reactive power while the active power output may be disabled (i.e.,  $I_q = I_N$ ). In that case, the system might still operate at *Const.-P* mode, depending on the inverter current limitation, and the current in the  $dq$ -frame is given by

$$\begin{cases} I_d = \frac{k_d}{v_g} I_N \\ I_q = I_N. \end{cases} \quad (6)$$

However, when the required injection of reactive power is fulfilled, according to (3), it might pose the inverter at a risk of overcurrent and, thus, overheating with this control strategy to maintain a constant output power (i.e., maximum power with MPPT control). Thus, based on (5) and (6), the following constraints should be satisfied in order to avoid inverter shutdown during LVRT:

$$\frac{1}{v_g} \sqrt{k_d^2 + k^2 (v_g - v_g^2)^2} \leq \frac{I_{\max}}{I_N} \quad (7)$$

when  $(1 - (1/k))$  p.u.  $\leq v_g < 0.9$  p.u., and

$$\frac{1}{v_g} \sqrt{k_d^2 + v_g^2} \leq \frac{I_{\max}}{I_N} \quad (8)$$

when  $v_g < (1 - (1/k))$  p.u. Those could be the design criterions for component selection and can be illustrated in Fig. 5.

It is observed in Fig. 5 that the minimum value of the inverter current limitation ( $I_{\max}$ ) should be  $2.24 I_N$  when  $k = 2$  p.u. so that the RPI strategy can be adopted in case of a wide range of voltage drop (i.e., the grid voltage is within  $0.5$  p.u.  $\leq v_g < 0.9$  p.u.) without power derating ( $k_d = 1$  p.u.). As for a predesigned PV inverter with a robustness margin, the system

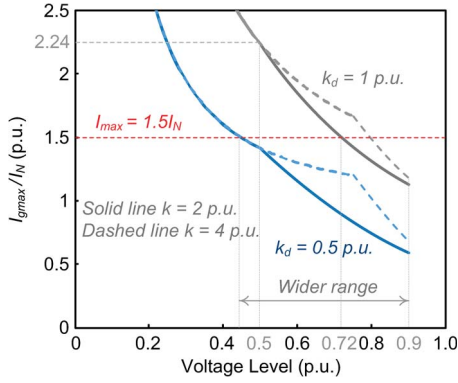


Fig. 5. Design constraint of the *Const.-P* considering the inverter overcurrent protection, where  $k_d = P/P_N$  and  $k$  is defined in (1).

has to derate the output power in order to inject enough reactive power. For example, if the allowable maximum current of a PV inverter  $I_{\max} = 1.5I_N$  and  $k = 2$  p.u., the PV systems should reduce the active power output (e.g.,  $k_d = 0.5$  p.u.) when the voltage drops below 0.72 p.u., as shown in Fig. 5. It is also noted in Fig. 5 that, by derating operation, the *Const.-P* strategy can be adopted for a wider range of voltage sags.

### B. Constant Active Current Control (*Const.-I<sub>d</sub>*)

Another RPI control possibility under LVRT operation is to keep the active current constant (i.e.,  $I_d = \text{const.}$ ). According to (4), the active current  $I_d$  can be obtained as

$$I_d = \frac{2P}{v_{gm}} = mI_N = \text{const.} \quad (9)$$

in which  $m$  is defined as the scaling factor for the design consideration in case of derating operations and  $0 \leq m \leq 1$  p.u. According to (9), the active power will automatically be reduced when this RPI control strategy is adopted in the response to voltage sags, i.e.,  $P \propto v_{gm}$ . Meanwhile, the reactive current  $I_q$  can be calculated according to the requirement shown in Fig. 4(a) and (2). Subsequently, the current in the  $dq$ -frame can be given as

$$\begin{cases} I_d = mI_N \\ I_q = k(1 - v_g)I_N \end{cases} \quad (10)$$

where  $(1 - (1/k))$  p.u.  $\leq v_g < 0.9$  p.u. and  $k$  are defined previously. Notably, when a severe voltage fault happens (very low voltage), the PV system should inject full reactive power. In that case, the current in the  $dq$ -frame can be expressed as

$$\begin{cases} I_d = mI_N \\ I_q = I_N \end{cases} \quad (11)$$

when  $v_g < (1 - (1/k))$  p.u.

With the *Const.-I<sub>d</sub>* control strategy, the amplitude of the injected current may also exceed the inverter limitation according to (3) and then trip the inverter protection. In order to avoid this, the following conditions should be fulfilled:

$$\sqrt{m^2 + k^2(1 - v_g)^2} \leq \frac{I_{\max}}{I_N} \quad (12)$$

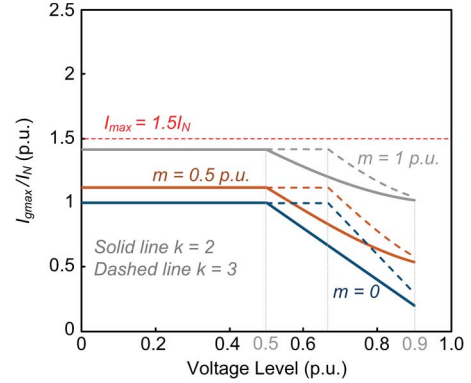


Fig. 6. Design constraint of the *Const.-I<sub>d</sub>* considering the inverter overcurrent protection, where  $m = I_d/I_N$  and  $k$  is defined in (1).

when  $(1 - (1/k))$  p.u.  $\leq v_g < 0.9$  p.u., and

$$\sqrt{m^2 + 1} \leq \frac{I_{\max}}{I_N} \quad (13)$$

when  $v_g < (1 - (1/k))$  p.u. For simplicity, the level of active current can be controlled to be that of the rated current (i.e.,  $m = 1$  p.u., and  $I_d = I_N$ ).

Similarly, a design guide for this RPI control strategy can be given in Fig. 6. It is seen from Figs. 5 and 6 that the PV inverter with *Const.-I<sub>d</sub>* control can be designed with a lower  $I_{\max}/I_N$  when it is compared to the one with a *Const.-P* control strategy. Therefore, it offers the possibility to select power devices with lower current ratings and, thus, lower cost. It is also worth to point out that the derating operation of a PV system can be achieved by changing  $m$  because of the proportional relationship between the active power and the grid voltage amplitude,  $P \propto v_{gm}$ . A smaller  $m$  leads to the possibility to select power devices of further lower ratings.

### C. Constant Peak Current Control (*Const.-I<sub>gmax</sub>*)

A PV inverter with the previous discussed RPI strategies has a risk of overcurrent loading when it is operating in LVRT mode. Thus, the *Const.-I<sub>gmax</sub>* is proposed. With this control strategy, there is no unintentional inverter shutdown due to overcurrent protection since the peak of the injected grid current is kept constant and lower than the inverter current limitation during LVRT, i.e.,  $I_{g\max} = nI_N = \text{const.}$ , and  $I_{g\max} \leq I_{\max}$ , where  $n$  is defined as the peak current scaling factor. According to (2), when the grid voltage is within the range  $(1 - (1/k))$  p.u.  $\leq v_g < 0.9$  p.u., the current in the  $dq$ -frame can be given by

$$\begin{cases} I_d = \sqrt{n^2 - k^2(1 - v_g)^2}I_N \\ I_q = k(1 - v_g)I_N \end{cases} \quad (14)$$

while if the grid voltage goes further lower than  $(1 - (1/k))$  p.u., according to (3), the current in the  $dq$ -frame should be

$$\begin{cases} I_d = \sqrt{n^2 - 1}I_N \\ I_q = I_N \end{cases} \quad (15)$$

where  $v_g$  and  $k$  are defined previously.

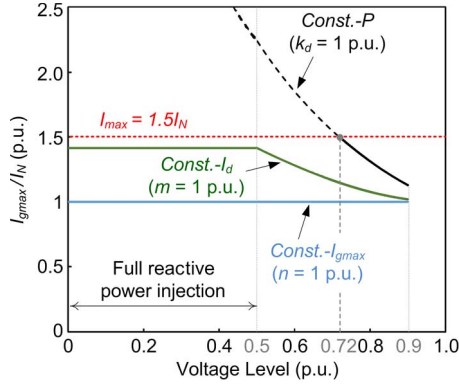


Fig. 7. Application conditions for three RPI strategies under different grid voltage levels for the case when  $k = 2$  p.u. and  $I_{\max} = 1.5I_N$ .

It should be noted that  $n$  has a maximum value of  $I_{\max}/I_N$  p.u., considering the inverter current protection shown in (3). For example, when an inverter is designed with a margin of 2 p.u. (i.e.,  $I_{\max} = 2I_N$ ), the maximum  $n$  should be 2 p.u. to ensure a stable RPI without tripping the inverter during LVRT. Thus, if  $n \leq (I_{\max}/I_N)$ , the riding-through operation of the PV inverter will not give an amplitude rise to the injected grid current. Meanwhile, according to (4) and (14), the active power will be reduced in order to inject sufficient reactive power during LVRT.

As mentioned earlier, the application conditions of the three proposed RPIs that complied with (2) are dependent of several parameters— $k$ ,  $k_d$ ,  $m$ ,  $n$ , and  $I_{\max}/I_N$ . Fig. 7 shows a comparison of three RPI strategies for a PV inverter with  $I_{\max} = 1.5I_N$  when  $k = 2$  p.u. It can be observed in Fig. 7 that the *Const.- $I_{g\max}$*  can be used in a wide range of voltage levels ( $0 \leq v_g < 0.9$  p.u.) even when  $k$  is different. This is the same case when the *Const.- $I_d$*  is adopted, as also proved by Fig. 6. In contrast, the *Const.- $P$*  is only in effectiveness within a certain range of grid voltage levels if without power derating operations ( $k_d = 1$  p.u.). For example, when the voltage level goes below 0.72 p.u. in the exemplified PV inverter, the RPI strategy should be changed to either *Const.- $I_d$*  or *Const.- $I_{g\max}$* , or derating operations have to be enabled as shown in Fig. 5; otherwise, the inverter will be tripped off due to overcurrent protection. Notably, as shown in Fig. 7, all three RPI strategies have to inject full reactive current in case of a severe voltage sag (e.g.,  $v_g < (1 - (1/k))$  p.u.) according to (2) and Fig. 4(a).

#### D. Thermal Optimized Control Strategy (*T-Optimized*)

High efficiency and high reliability have become of intense importance for next-generation PV inverters in order to reduce the cost of energy [10], [44]–[46]. In respect to reliability, possibilities to improve it can be achieved by considering rated power, packaging technologies, severe users, and harsh operation conditions, e.g., under grid faults [44]–[47]. However, as exemplified in a model of (16), the junction temperatures, including mean junction temperature  $T_{j-m}$  and temperature swings  $\Delta T_j$ , have a significant impact on the number of cycles to failure  $N_f$  of a power device [48]

$$N_f = \alpha(\Delta T_j)^{\beta_1} e^{\frac{\beta_2}{T_{j-m}}} (t_{ON})^{\beta_3} \cdot (\text{other factors}) \quad (16)$$

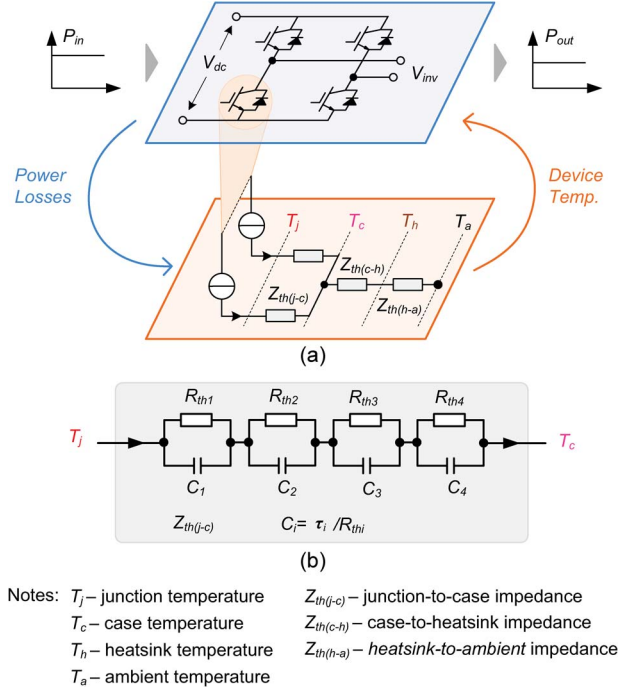


Fig. 8. (a) Electrical and thermal models of a power module and (b) Foster model of the thermal impedance from junction to case [47], [51], [52].

with  $t_{ON}$  being the pulse length and  $\alpha$  and  $\beta_{1,2,3}$  being the coefficients related to the device material, which can be obtained by means of curve fitting using numerical simulation or experimental accelerating tests [49]. According to Miner's rules [44], [45], [48]–[50], the power device lifetime is linearly dependent on temperature stress damage (i.e.,  $N_f$ ). Calculations of  $N_f$  based on the temperature profiles have been presented in [44] and [45] in detail. Those studies have shown that the junction temperature affects the entire system reliability. Since the thermal behavior of the power devices is coupled with the power losses, as shown in Fig. 8, the appropriate allocation of the active power and reactive power offers the controllability of the junction temperature.

For example, in LVRT operation, the injected reactive power is dependent on the voltage sag level, and also, as shown in (2) and Fig. 4(a),  $k$  is variable. Both will lead to a redistribution of power losses on the power devices, and also the thermal distribution. Therefore, a constant junction temperature (or at least cooled down junction temperature) of the power devices, and thus improved overall reliability, can be achieved by changing the RPI strategies and/or the slope  $k$  shown in Fig. 4(a). For instance, as shown in Fig. 9, a 0.3-p.u. voltage sag (i.e.,  $v_g = 0.7$  p.u.) occurs, and the *Const.- $I_{g\max}$*  is first activated. By adjusting the value  $k$  to 3 p.u., the operation points will change from *C* to *D*, while by changing the RPI strategy to *Const.- $P$* , the operation point will correspondingly move from *C* to *A*.

This is the operation principle of the *T-optimized* control strategy in LVRT applications. As for the implementation of the *T-optimized* control strategy, one essential part is to create the power reference unit according to voltage sag depths. One method is based on the mathematical derivations, and an alternative is based on lookup tables, which has been adopted in

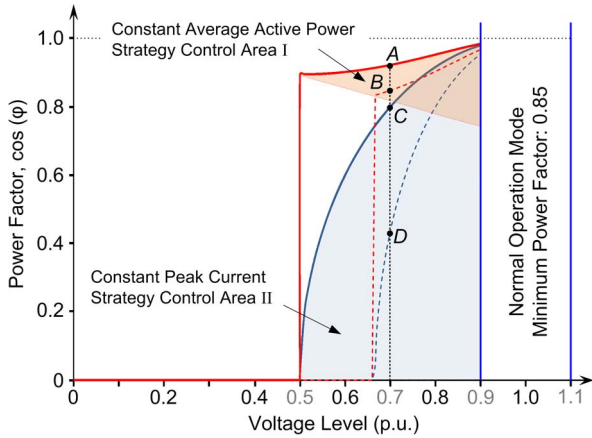


Fig. 9. Power factor curves versus voltage levels for different control strategies. Solid lines:  $k = 2$ . Dashed lines:  $k = 3$ .  $k$  is defined in (1).

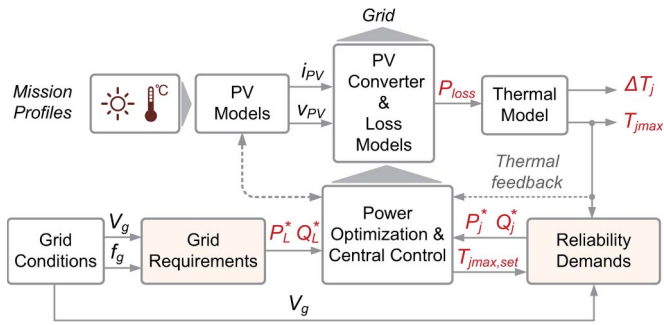


Fig. 10. Control structure of the  $T$ -Optimized strategy for single-phase PV systems.

this paper. The lookup table-based power reference model can simply be given as

$$T_{j \max} = f(P_j, Q_j). \quad (17)$$

A detailed implementation of this control strategy is shown in Fig. 10, which implies that the  $T$ -optimized strategy complies with both the RPI requirement in LVRT (performed by “Grid Requirements” unit) and improved reliability demand (performed by “Reliability Demands” unit). In normal operation mode, since a minimum power factor is required, the system directly sets the references ( $P^* = P_{MPP}$  and  $Q^* = 0$  var) for the central control unit, as shown in Fig. 11, while in the case of a voltage sag, both control units will send out the power references ( $P_L^*$  and  $Q_L^*$ ,  $P_j^*$  and  $Q_j^*$ ) and, then, the central control unit will optimize the power to achieve both goals. Notably, as shown in Fig. 11, in order to achieve a reduced or constant junction temperature, there might be several sets of power references as long as the power losses are reduced or kept constant, according to Fig. 8. In that case, optimization objectives, e.g.,  $P^* = \max\{P_1^*, P_2^*, \dots\}$ , can be applied to determine the power references for the central control unit.

In terms of application conditions for the  $T$ -optimized control strategy, it is mainly dependent on the maximum junction temperature reference  $T_{j \max, set}$ , on the assumption that the system is operating at nominal conditions before failure and the maximum junction temperature is  $T_{j \max, 0}$ . If the grid voltage sags to lower than  $(1 - (1/k))$  p.u., the  $T$ -optimized control

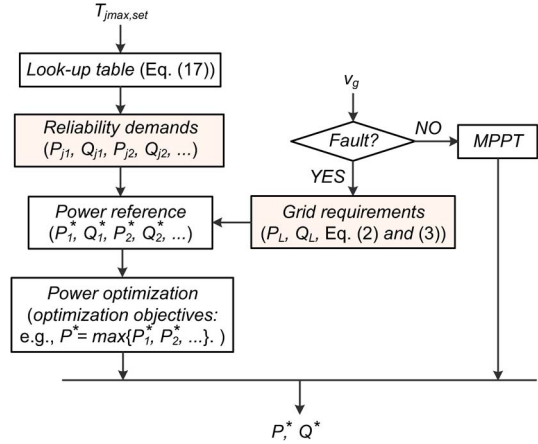


Fig. 11. Flowchart of the  $T$ -optimized control strategy.

strategy can be applied to realize a controllable junction temperature with  $T_{j \max, set} \geq T_{j \max, 0}$ , while a reduced junction temperature (i.e.,  $T_{j \max, set} < T_{j \max, 0}$ ) cannot be achieved. When the grid voltage is within the range  $(1 - (1/k))$  p.u.  $\leq v_g < 0.9$  p.u., the junction temperature can be controlled either lower than that before failure (i.e.,  $T_{j \max, set} < T_{j \max, 0}$ ) or at a certain level (e.g.,  $T_{j \max, set} = T_{j \max, 0}$ ), depending on the voltage sag depth. It should be noted that, in case of overcurrent protection (or overheating protection), the temperature reference should satisfy this condition:  $T_{j \max, set} \leq T_{j \max, inv}$ , with  $T_{j \max, inv}$  being the allowable maximum junction temperature of the power devices.

However, it should be pointed out that a voltage fault normally is a very short-term event, and thus, the  $T$ -optimized control strategy may not take a fast and effective response to the voltage sag during this time interval, yet on the one hand, the idea of thermal optimization by reallocating the active power and reactive power can be adopted in the power electronics-based systems in order to achieve improved reliability and, thus, a reduced cost of energy, particularly if a wide range of reactive power injection is allowed by future grid codes. On the other hand, the  $T$ -optimized strategy is also designed to limit the maximum junction temperature since catastrophic failures may occur due to a short-term single event (e.g., LVRT) of overtemperature, and thus overheating, which exceeds the limit of the insulated-gate bipolar transistor (IGBT) power devices.

### E. Benchmarking of the Proposed RPI Strategies

During the design and the operation of the PV inverters, those aforementioned constraints should be considered. In particular, for the next-generation PV systems, the provision of reactive power as an advanced feature both in normal operation and under grid faults, and the requirements of LVRT will come into force in the near future. The corresponding active and reactive power references under different voltage sag levels for the proposed RPI control strategies can be obtained based on the aforementioned discussions. Thus, the required reactive power complying with grid codes can be injected. A benchmarking of the proposed RPI strategies is summarized in Table I, which shows the advantages and design constraints/considerations of each RPI control strategy.

TABLE I  
 BECHMARKING OF THE PROPOSED REACTIVE POWER INJECTION STRATEGIES

RPI Strategy	Advantages	Design Constraints	Remarks
<i>Const.-P</i>	<ul style="list-style-type: none"> <li>Maximized energy yield (with MPPT control)</li> </ul>	<ul style="list-style-type: none"> <li>Over-current trip-off</li> <li>Derating operation is necessary under severe faults</li> <li>Large design margin for a wide voltage range</li> </ul>	It requires a very large design margin for the power devices, and thus cost increases, especially under deep voltage sags.
<i>Const.-I<sub>d</sub></i>	<ul style="list-style-type: none"> <li>Reduced power operation (<math>P \propto v_g</math>)</li> </ul>	<ul style="list-style-type: none"> <li>Over-current issues</li> <li>May also require power derating operation</li> <li>Small design margin for a wide voltage range</li> </ul>	For new-design inverters, it has lower rating requirements for the power devices compared to <i>Const.-P</i> .
<i>Const.-I<sub>gmax</sub></i>	<ul style="list-style-type: none"> <li>No over-current problems</li> <li>Applicable for all inverters</li> </ul>	—	No current amplitude rise. This strategy is applicable for all predesigned PV inverters.
<i>T-Optimized</i>	<ul style="list-style-type: none"> <li>Compliance with both LVRT and reliability requirements</li> </ul>	<ul style="list-style-type: none"> <li>Increased implementation complexity</li> </ul>	It is a hybrid solution between the above three strategies. Improvement of reliability can be achieved by reallocating reactive and active powers.

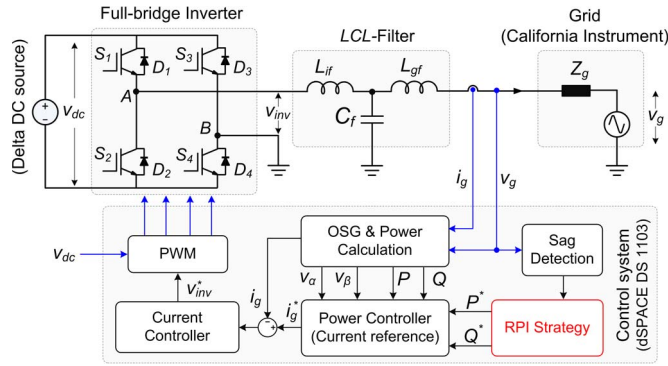


Fig. 12. Hardware schematic and overall control structure of a single-phase grid-connected system with RPI control strategies.

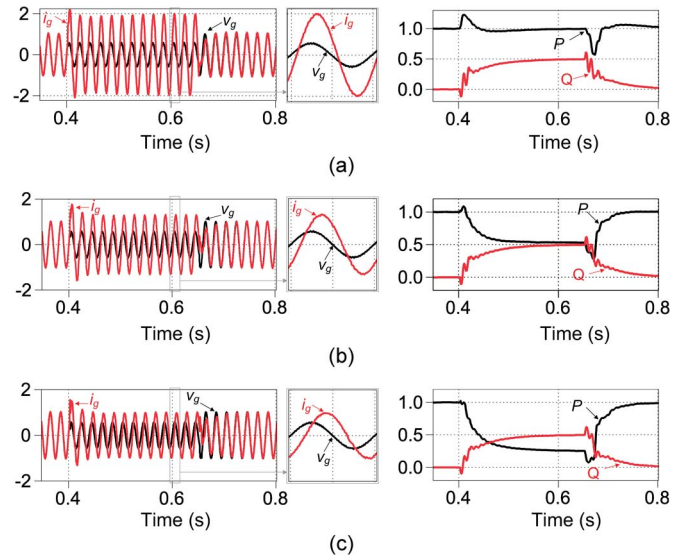
It can be seen from the benchmarking results that those RPI strategies can fulfill the grid requirements but with different control objectives. The first two strategies are designed with the purpose to produce as much energy as possible during LVRT. Moreover, the *Const.-I<sub>d</sub>* control strategy requires a lower power rating for the inverter compared to the *Const.-P* strategy, while the *Const.-I<sub>gmax</sub>* maintains a constant peak current and thus can be implemented in any predesigned PV inverter. The *T-Optimized* strategy is a hybrid alternative considering the RPI and reliability requirements for PV inverters. According to Table I, a combination of the proposed strategies is an inspiring way to cost-effectively design new PV inverters when considering the inverter VA ratings, power production capability, control complexity, and also the occurrence rate of grid voltage sags.

#### IV. SIMULATION AND EXPERIMENTAL RESULTS

Referring to Figs. 2 and 3, simulation and experimental tests were carried out to demonstrate the effectiveness of the proposed RPI strategies. Fig. 12 shows the hardware configuration of a single-phase system used for the verifications, and it also shows that the RPI control is triggered by the detected voltage fault (e.g., grid voltage level  $v_g$ ). System parameters are listed in Table II. In both simulations and experiments, a proportional resonant current controller with harmonic compensators is adopted to maintain a satisfactory power quality, as shown in Fig. 3.

 TABLE II  
 SIMULATION AND EXPERIMENTAL PARAMETERS

Nominal grid voltage amplitude	$v_{gmn} = 325.2$ V
Nominal grid frequency	$\omega_0 = 2\pi \times 50$ rad/s
Grid impedance	$L_g = 4$ mH, $R_g = 0.2$ $\Omega$
LCL-filter	$L_{if} = 3.6$ mH, $C_f = 2.35$ $\mu$ F, $L_{gf} = 708$ $\mu$ H
Sampling and switching frequency	$f_s = f_{sw} = 10$ kHz
DC voltage	$V_{dc} = 400$ V


 Fig. 13. Performance of a 1-kW single-phase PV system in LVRT operation mode with three different RPI control strategies ( $i_g$ ,  $v_g$ —grid current and voltage [p.u.];  $P$ ,  $Q$ —average active power and reactive power [p.u.]; voltage level:  $v_g = 0.55$  p.u.;  $k = 2$  p.u.): (a) *Const.-P* with  $k_d = 1$  p.u., (b) *Const.-I<sub>d</sub>* with  $m = 1$  p.u., and (c) *Const.-I<sub>gmax</sub>* with  $n = 1$  p.u.

##### A. Simulation Results

Simulations are first carried out, and a voltage sag of 0.45 p.u. is generated (i.e.,  $v_g = 0.55$  p.u. during LVRT operation). Fig. 13 shows the performance of a 1-kW single-phase system with *Const.-P*, *Const.-I<sub>d</sub>*, and *Const.-I<sub>gmax</sub>* RPI strategies in LVRT. Based on the thermal models in Fig. 8 and thermal parameters of the IGBT module (see Table III), the same single-phase system with the *T-optimized* RPI control strategy is also simulated, and the results are given in Figs. 14 and 15.

TABLE III  
THERMAL PARAMETERS OF THE IGBT MODULE FROM  
A LEADING MANUFACTURER FOR THE SIMULATIONS

Impedance		$Z_{th(j-c)}$ , Junction-to-case temp.			
	$i$	1	2	3	4
IGBT	$R_{thi}$ (K/W)	0.074	0.173	0.526	0.527
	$\tau_i$ (s)	0.0005	0.005	0.05	0.2
Diode	$R_{thi}$ (K/W)	0.123	0.264	0.594	0.468
	$\tau_i$ (s)	0.0005	0.005	0.05	0.2

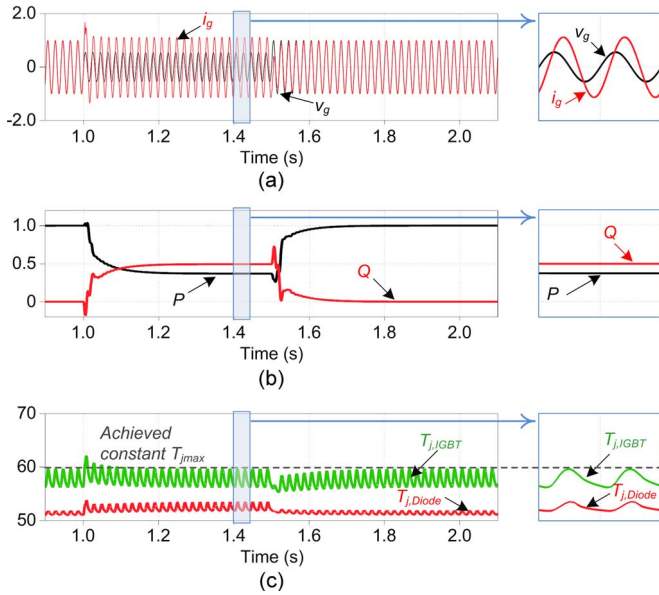


Fig. 14. Simulation results of a 1-kW single-phase grid-connected PV system with  $T$ -optimized control strategy ( $k = 2$  p.u.): (a) Grid current  $i_g$  and voltage  $v_g$  [p.u.], (b) active power  $P$  and reactive power  $Q$  [p.u.], and (c) junction temperature  $T_j$  [°C]; voltage level:  $v_g = 0.55$  p.u.

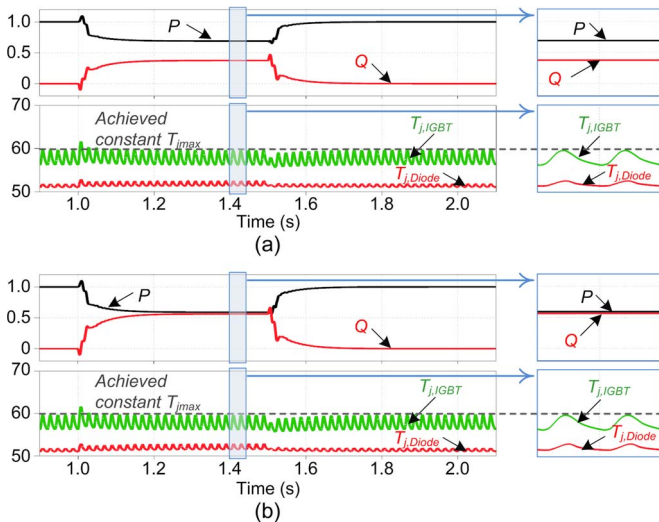


Fig. 15. Performance of a 1-kW single-phase PV inverter with  $T$ -optimized strategy under grid faults (active power  $P$  and reactive power  $Q$  [p.u.]; junction temperature  $T_j$  [°C];  $v_g = 0.75$  p.u.): (a)  $k = 2$  p.u. and (b)  $k = 3$  p.u.

When the voltage sag is detected, the system goes into LVRT operation mode, and the system injects the required reactive power to support the voltage according to Fig. 4(a). At the same

time, the active power is also controlled in order to achieve different objectives according to (5), (10), and (14), i.e., to inject the maximum active power during fault ride-through, to keep the active current constant, and to maintain the peak current, as shown in Fig. 13. It can also be observed in Fig. 13(a) that, although the  $Const.-P$  can maximize the power output during LVRT operation, it also gives a large amplitude rise of the injected current, which may trigger the inverter overcurrent protection (i.e., fail to ride-through grid faults). This is the same in case the  $Const.-I_d$  strategy is adopted in LVRT operation mode as indicated in Fig. 13(b). However, the amplitude increase in the  $Const.-I_d$  controlled system is smaller in contrast with that in the  $Const.-P$  controlled system. Moreover, since the peak of the injected current is maintained constant during LVRT as shown in Fig. 13(c), the  $Const.-I_{g,max}$  strategy can operate under a wide range of voltage levels without overcurrent issues. Those results are in consistency with the previous discussions.

Notably, with the  $T$ -optimized control strategy, the junction temperature of IGBT power devices is maintained constant, as shown in Figs. 14(c) and 15, while sufficient reactive power is also injected to the grid according to Fig. 4(a). Hence, both required reactive power support and improved reliability are achieved. It is also indicated in Fig. 15 that the constant maximum junction temperature can be achieved by changing  $k$  under grid faults. This is also in accordance with the previous discussions, viz., (17) may have several solutions ( $P_{j1}, Q_{j1}, P_{j2}, Q_{j2}, \dots$ ). Hence, the optimization objectives should be applied to determine the power references for the control system according to Fig. 11.

When comparing the levels of the injected grid current with different control strategies shown in Figs. 13 and 14(a), it can be found that the  $Const.-I_{g,max}$  can achieve the lowest current level, and then, the junction temperature of the power devices with this RPI strategy is also lower. The analysis has been proved by the results presented in Fig. 16. Since another objective of the  $T$ -optimized strategy is to maintain a constant maximum junction temperature considering the overall reliability, more active power is injected during fault ride-through as shown in Fig. 14(b). By further reducing the active power injection but providing sufficient reactive power during LVRT, a reduced maximum junction temperature can be achieved, which is another case of the  $T$ -optimized strategy. This also verified the controllability of junction temperature of the power devices through appropriate allocations of the active power and the reactive power. Nevertheless, it is also observed in Fig. 16 that all the RPI strategies, except for the  $Const.-P$ , can limit the maximum junction temperature to some extent, and thus, catastrophic failures are avoided.

## B. Experimental Tests

In the experimental verifications, a voltage sag of 120 ms has been programmed in an ac power source. The  $Const.-P$  control strategy has been tested first on a 1-kW single-phase grid-connected system under a severe voltage sag (0.45 p.u., i.e.,  $v_g = 0.55$  p.u.). A commercial inverter with the rated current of 5 A in rms has been used as the conversion stage. If a severe

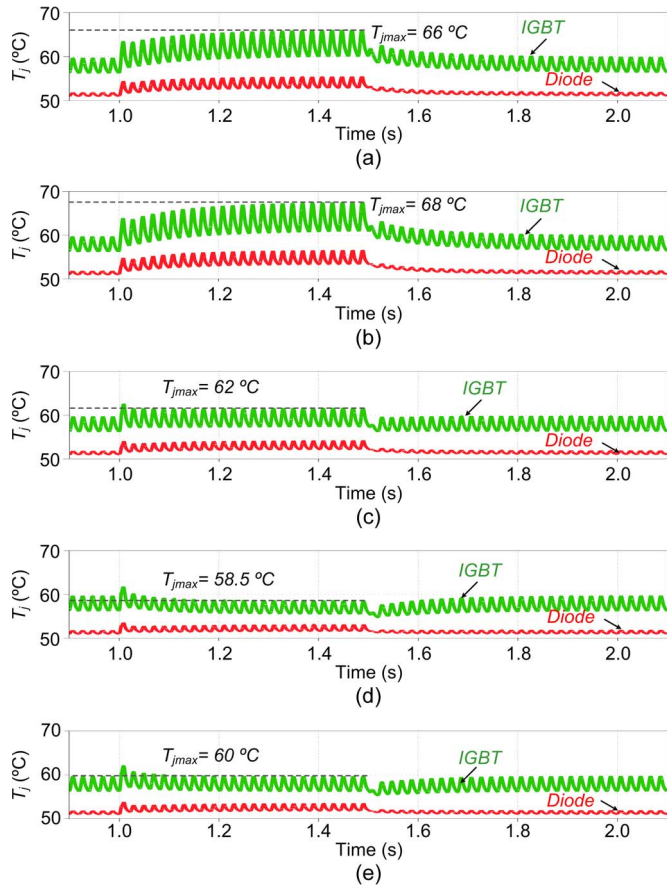


Fig. 16. Junction temperature ( $T_j$ ) of the power devices in a 1-kW single-phase PV inverter under grid faults (voltage level  $v_g = 0.55$  p.u. and  $k = 2$  p.u.): (a) Without LVRT, (b) *Const.-P* with  $k_d = 1$  p.u., (c) *Const.-I<sub>d</sub>* with  $m = 1$  p.u., (d) *Const.-I<sub>gmax</sub>* with  $n = 1$  p.u., and (e) *T-optimized*.

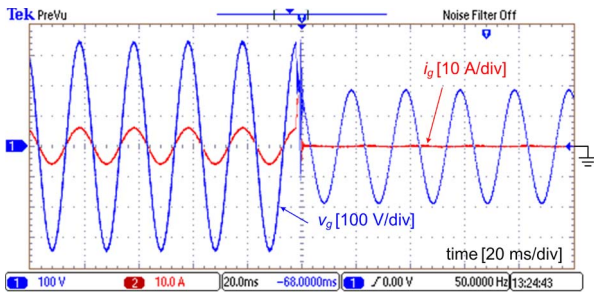


Fig. 17. Overcurrent protection of a single-phase inverter with *Const.-P* control (voltage level  $v_g = 0.55$  p.u.,  $k_d = 1$  p.u., and  $k = 2$  p.u.).

voltage fault (e.g., 0.45 p.u.) happens, the amplitude of the injected grid current may exceed the current limitation, and consequently, the inverter will be tripped off, as it has been verified by the experimental results shown in Fig. 17. One possibility of riding-through fault operation is to reduce the output power (i.e., power derating operation) as discussed previously. Here, in the experimental results shown in Fig. 18, the voltage presents a 0.20 p.u. voltage sag (i.e.,  $v_g = 0.8$  p.u.) in order to test the performance of the *Const.-P* control strategy, and thus, the system can operate under this grid fault without derating active power. At the same time, sufficient reactive power is injected to the grid according to Fig. 4(a).

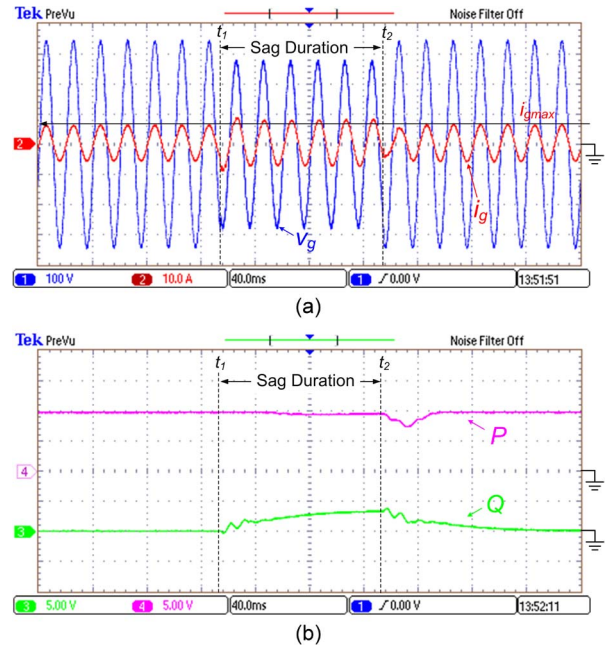


Fig. 18. Experimental results of a single-phase system with the *Const.-P* RPI control strategy (voltage level  $v_g = 0.8$  p.u.,  $k_d = 1$  p.u., and  $k = 2$  p.u.): (a) Grid voltage  $v_g$  [100 V/div] and grid current  $i_g$  [10 A/div]; (b) active power  $P$  [500 W/div] and reactive power  $Q$  [500 var/div]; time [40 ms/div].

In contrast with the simulation results, the *Const.-I<sub>gmax</sub>* and *Const.-I<sub>d</sub>* control strategies are tested under the severe voltage sag (0.45 p.u.) on the same single-phase grid-connected system. The performance of the system under such a voltage sag is shown in Fig. 19. The results demonstrate that the *Const.-I<sub>gmax</sub>* control strategy can contribute to a constant amplitude of the injected current and thus prevent the inverter from overcurrent tripping during LVRT. At the same time, an injection of appropriate reactive power according to the requirements shown in Fig. 4(a) is ensured by this control strategy. Similarly, the *Const.-I<sub>d</sub>* RPI strategy can inject sufficient reactive power, which is dependent on the voltage sag level, and the active current is maintained constant during LVRT, while the injected current amplitude is slightly larger than that in the system with *Const.-I<sub>gmax</sub>* control. As a consequence, depending on the inverter design margin, this may also trip off the inverter during LVRT. Nonetheless, the aforementioned presented results have verified the effectiveness of the proposed RPI strategies for single-phase PV systems as long as the design constraints are taken into account.

A constant power loss before, during, and after the LVRT operation could achieve a constant temperature operation. Since the junction temperature measurement under full loading condition is challenging and is still an ongoing research topic in the semiconductor area [53], this paper experimentally measures the power losses of the IGBTs under different control strategies, which can indirectly reveal their thermal stresses. Fig. 20 shows the performance of a single-phase PV system (higher  $I_{max}/I_N$ ) under a grid voltage sag. It can be seen in Fig. 20 that the *T-Optimized* RPI strategy can inject appropriate reactive power as what the other RPI strategies can do. In contrast, the *T-Optimized* strategy can also achieve a desirable (optimized) junction temperature of the power devices.

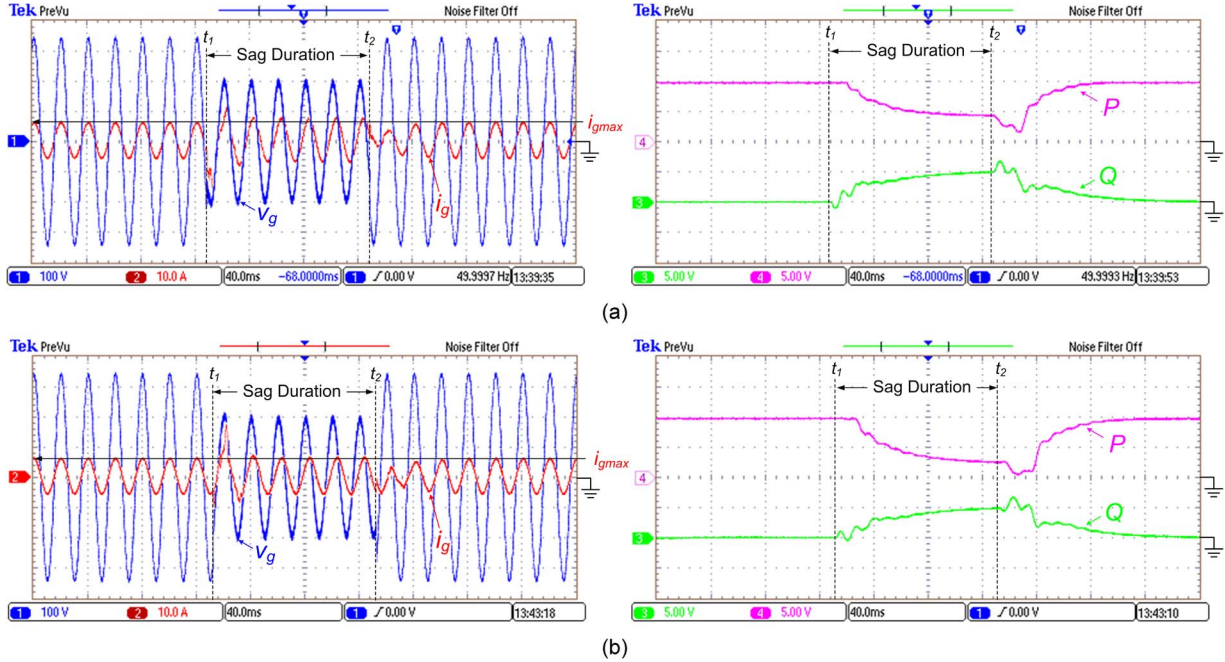


Fig. 19. Experimental results of a single-phase grid-connected system with different RPI control strategies (voltage level  $v_g = 0.55$  p.u.,  $k = 2$  p.u., grid voltage  $v_g$  [100 V/div], grid current  $i_g$  [10 A/div], active power  $P$  [500 W/div], reactive power  $Q$  [500 var/div], and time [40 ms/div]): (a) *Const.-I<sub>d</sub>* with  $m = 1$  p.u. and (b) *Const.-I<sub>gmax</sub>* with  $n = 1$  p.u.

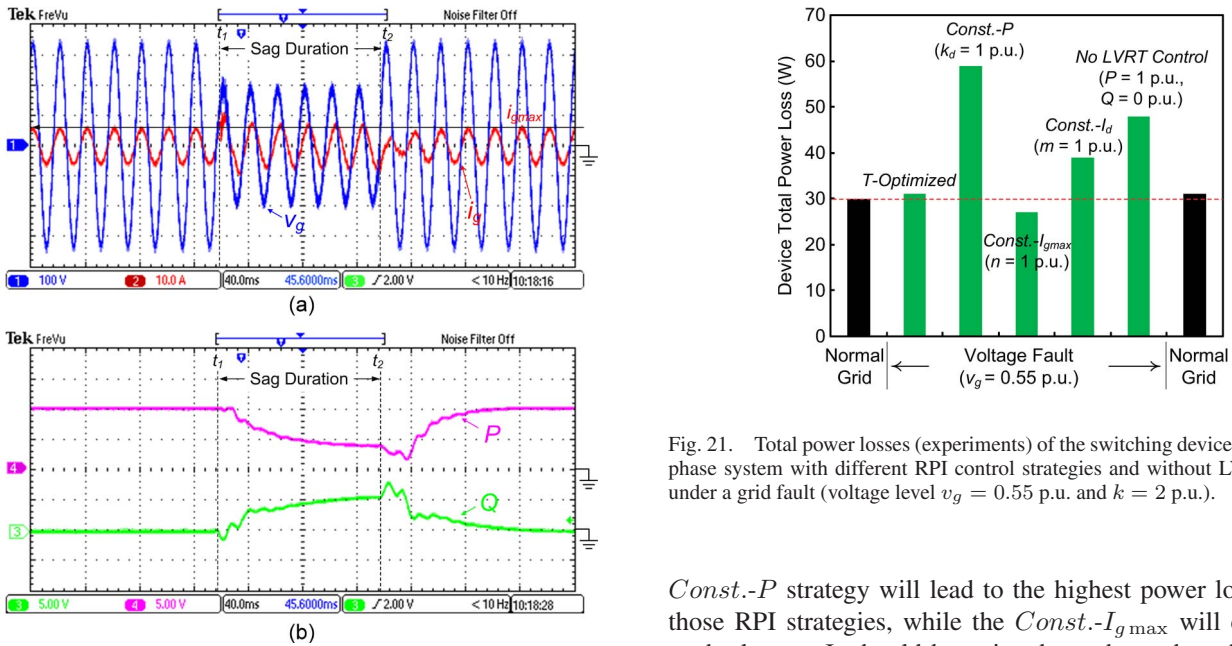


Fig. 20. Experimental results of a 1-kW single-phase system with *T-Optimized* RPI control strategy (voltage level  $v_g = 0.55$  p.u. and  $k = 2$  p.u.): (a) Grid voltage  $v_g$  [100 V/div] and grid current  $i_g$  [10 A/div]; (b) active power  $P$  [500 W/div] and reactive power  $Q$  [500 var/div]; time [40 ms/div].

This advantage has been indirectly verified by the results shown in Fig. 21, where the power losses are measured using a YOKOGAWA WT3000 Precision Power Analyzer. It can be seen from Fig. 21 that the *T-Optimized* strategy can achieve an almost constant power loss in contrast to that in unity power factor operation (before and after the voltage fault). The

Fig. 21. Total power losses (experiments) of the switching devices in a single-phase system with different RPI control strategies and without LVRT control under a grid fault (voltage level  $v_g = 0.55$  p.u. and  $k = 2$  p.u.).

*Const.-P* strategy will lead to the highest power loss among those RPI strategies, while the *Const.-I<sub>gmax</sub>* will contribute to the lowest. It should be pointed out that, when there is no LVRT control, the power loss will also increase drastically depending on the voltage sag level. According to the authors of [44], [45], and [47], the power losses will cause temperature rise at the device junction. This means that the *Const.-P* and the system without LVRT control might pose the inverter at a risk of overcurrent and also overtemperature. The *T-Optimized* control is able to maintain a constant temperature, and the *Const.-I<sub>gmax</sub>* can achieve the lowest junction temperature. Those results are in agreement with the results shown in Fig. 15 and have corroborated the effectiveness of the proposed RPI strategies in terms of thermal performance.

## V. CONCLUSION

In this paper, reactive power injection strategies for single-phase PV systems considering grid requirements have been explored. The proposed reactive power injection strategies include constant average active power control, constant active current control, constant peak current control, and thermal optimized reactive power control strategy, which is dedicated to improve the reliability during LVRT operation and to avoid catastrophic failures. All the discussed control strategies are in compliance with the grid codes currently defined for medium-voltage applications. The proposed reactive power control strategies have also been tested either by simulations or by experiments. The results show the effectiveness of the reactive power injection strategies to support the grid voltage during LVRT operation with different objectives, e.g., maximum output power (constant average active power control). Design constraints for those strategies have also been studied in this paper, and a benchmarking of the proposed strategies has been provided. It offers a feasible way to select appropriate power devices for the new PV inverters with the specific control strategy proposed in this paper.

As the future grid demands will be more stringent and the reactive power injection function is one of them, the PV systems serving even low-voltage grids have to comply with those requirements in both normal operation mode and under grid faults. The proposed control strategies can be implemented in those PV systems with the provided design guidelines. Hence, the control strategies can further accelerate the pace of advanced PV inverter development.

## REFERENCES

- [1] C. Winneker, World's Solar Photovoltaic Capacity Passes 100-Gigawatt Landmark After Strong Year, Feb. 2013. [Online]. Available: <http://www.epia.org/news/>
- [2] D. Rosenwirth and K. Strubbe, Integrating Variable Renewables as Germany Expands Its Grid, Mar. 2013. [Online]. Available: <http://www.renewableenergyworld.com/>
- [3] European Photovoltaic Industrial Association, Global Market Outlook for Photovoltaics Until 2016, 2012. [Online]. Available: <http://www.epia.org/>
- [4] Y. Bae, T.-K. Vu, and R.-Y. Kim, "Implemental control strategy for grid stabilization of grid-connected PV system based on German grid code in symmetrical low-to-medium voltage network," *IEEE Trans. Energy Convers.*, vol. 28, no. 3, pp. 619–631, Sep. 2013.
- [5] "Renewables 2013: Global Status Report (GSR)," Paris, France, Jun. 2013. [Online]. Available: <http://www.ren21.net/>
- [6] S. B. Kjaer, J. K. Pedersen, and F. Blaabjerg, "A review of single-phase grid-connected inverters for photovoltaic modules," *IEEE Trans. Ind. Appl.*, vol. 41, no. 5, pp. 1292–1306, Sep./Oct. 2005.
- [7] F. Blaabjerg, R. Teodorescu, M. Liserre, and A. V. Timbus, "Overview of control and grid synchronization for distributed power generation systems," *IEEE Trans. Ind. Electron.*, vol. 53, no. 5, pp. 1398–1409, Oct. 2006.
- [8] Y. Yang, F. Blaabjerg, and Z. Zou, "Benchmarking of grid fault modes in single-phase grid-connected photovoltaic systems," *IEEE Trans. Ind. Appl.*, vol. 49, no. 5, pp. 2167–2176, Sep./Oct. 2013.
- [9] E. Romero-Cadaval *et al.*, "Grid-connected photovoltaic generation plants: Components and operation," *IEEE Ind. Electron. Mag.*, vol. 7, no. 3, pp. 6–20, Sep. 2013.
- [10] Y. Yang, P. Enjeti, F. Blaabjerg, and H. Wang, "Suggested grid code modifications to ensure wide-scale adoption of photovoltaic energy in distributed power generation systems," in *Conf. Rec. IEEE IAS Annu. Meeting*, Oct. 6–11, 2013, pp. 1–8.
- [11] R. Carnieletto, D. I. Brandão, F. A. Farret, M. G. Simões, and S. Suryanarayanan, "Smart grid initiative: A multifunctional single-phase voltage source inverter," *IEEE Ind. Appl. Mag.*, vol. 17, no. 5, pp. 27–35, 2011.
- [12] R. Teodorescu, M. Liserre, and P. Rodriguez, *Grid Converters for Photovoltaic and Wind Power Systems*. Hoboken, NJ, USA: Wiley, 2011.
- [13] M. Ciobotaru, R. Teodorescu, and F. Blaabjerg, "Control of single-stage single-phase PV inverter," in *Proc. EPE*, 2005, pp. P.1–P.10.
- [14] S. Jain and V. Agarwal, "A single-stage grid connected inverter topology for solar PV systems with maximum power point tracking," *IEEE Trans. Power Electron.*, vol. 22, no. 5, pp. 1928–1940, Sep. 2007.
- [15] D. Maxwell, "Parts of Northern Ireland's electricity grid overloaded," BBC News, Nov. 13, 2013. [Online]. Available: <http://www.bbc.co.uk/>
- [16] E. J. Coster, J. M. A. Myrzik, B. Kruimer, and W. L. Kling, "Integration issues of distributed generation in distribution grids," *Proc. IEEE*, vol. 99, no. 1, pp. 28–39, Jan. 2011.
- [17] H. Gaztanaga *et al.*, "Enhanced experimental PV plant grid-integration with a MW lithium-ion energy storage system," in *Proc. ECCE*, Sep. 15–19, 2013, pp. 1324–1329.
- [18] G. Mokhtari, A. Ghosh, G. Nourbakhsh, and G. Ledwich, "Smart robust resources control in LV network to deal with voltage rise issue," *IEEE Trans. Sustain. Energy*, vol. 4, no. 4, pp. 1043–1050, Oct. 2013.
- [19] T. Stetz, F. Marten, and M. Braun, "Improved low voltage grid-integration of photovoltaic systems in Germany," *IEEE Trans. Sustain. Energy*, vol. 4, no. 2, pp. 534–542, Apr. 2013.
- [20] R. Caldon, M. Coppo, and R. Turri, "Distributed voltage control strategy for LV networks with inverter-interfaced generators," *Elect. Power Syst. Res.*, vol. 107, pp. 85–92, Feb. 2014.
- [21] M. Arnold, W. Friede, and J. Myrzik, "Challenges in future distribution grids—A review," in *Proc. ICREPQ*, Mar. 20–22, 2013, pp. 1–6.
- [22] Fraunhofer ISE, Recent Facts About Photovoltaics in Germany, May 28, 2014. [Online]. Available: <http://www.pv-fakten.de/>
- [23] VDE Verband der Elektrotechnik Elektronik Informationstechnik e.V., Power Generation Systems Connected to the Low-Voltage Distribution Network—Technical Minimum Requirements for the Connection to and Parallel Operation With Low-Voltage Distribution Networks, *VDE-AR-N 4105:2011-08*, Aug. 2011.
- [24] Comitato Elettrotecnico Italiano, Reference Technical Rules for Connecting Users to the Active and Passive LV Distribution Companies of Electricity, *CEI 0-21*, Dec. 2011.
- [25] Y. Chen, A. Luo, Z. Shuai, and S. Xie, "Robust predictive dual-loop control strategy with reactive power compensation for single-phase grid-connected distributed generation system," *IET Power Electron.*, vol. 6, no. 7, pp. 1320–1328, Aug. 2013.
- [26] A. Cagnano, E. De Tuglie, M. Liserre, and R. A. Mastromauro, "Online optimal reactive power control strategy of PV inverters," *IEEE Trans. Ind. Electron.*, vol. 58, no. 10, pp. 4549–4558, Oct. 2011.
- [27] C.-T. Lee, C.-W. Hsu, and P.-T. Cheng, "A low-voltage ride-through technique for grid-connected converters of distributed energy resources," *IEEE Trans. Ind. Appl.*, vol. 47, no. 4, pp. 1821–1832, Jul./Aug. 2011.
- [28] R. Meyer, A. Zlotnik, and A. Mertens, "Fault ride through control of medium-voltage converters with LCL filter in distributed generation systems," *IEEE Trans. Ind. Appl.*, vol. 50, no. 5, pp. 3448–3456, Sep./Oct. 2014.
- [29] G. Arnold, Challenges of Integrating Multi-GW Solar Power Into the German Distribution Grids, Aug. 2011. [Online]. Available: <http://www.iwes.fraunhofer.de/>
- [30] C. H. Benz, W. T. Franke, and F. W. Fuchs, "Low voltage ride through capability of a 5 kW grid-tied solar inverter," in *Proc. EPE/PEMC*, 2010, pp. T12-13–T12-20.
- [31] Bundesverband der Energie- und Wasserwirtschaft (BDEW), Technical Guideline: Generating Plants Connected to the Medium-Voltage Network, Jun. 2008.
- [32] S. B. Kjaer, J. Dannehl, F. Mecking, and J. Godbersen, "A 12 megawatt power plant with fully implemented ancillary services according to the German grid codes—The first results," in *Proc. EUPVSEC*, Sep. 5/6, 2011, pp. 3869–3873.
- [33] H. Kobayashi, "Fault ride through requirements and measures of distributed PV systems in Japan," in *Proc. IEEE-PES Gen. Meet.*, Jul. 22–26, 2012, pp. 1–6.
- [34] N. Papanikolaou, "Low-voltage ride-through concept in flyback inverter-based alternating current-photovoltaic modules," *IET Power Electron.*, vol. 6, no. 7, pp. 1436–1448, Aug. 2013.
- [35] Y. Miyamoto, "Technology for high penetration residential PV systems on a distribution line in Japan," in *Proc. 5th Int. Conf. Integr. Renew. Distrib. Energy Res.*, Dec. 4–6, 2012, pp. 1–27.
- [36] J. C. Vasquez, R. A. Mastromauro, J. M. Guerrero, and M. Liserre, "Voltage support provided by a droop-controlled multifunctional inverter," *IEEE Trans. Ind. Electron.*, vol. 56, no. 11, pp. 4510–4519, Nov. 2009.
- [37] S. A. Khajehoddin, M. Karimi-Ghartemani, A. Bakhshai, and P. Jain, "A power control method with simple structure and fast dynamic response for

- single-phase grid-connected DG systems," *IEEE Trans. Power Electron.*, vol. 28, no. 1, pp. 221–233, Jan. 2013.
- [38] X. Zong and P. W. Lehn, "Reactive power control of single phase grid tied voltage sourced inverters for residential PV application," in *Proc. IEEE IECON*, 2012, pp. 696–701.
- [39] C.-H. Chang, Y.-H. Lin, Y.-M. Chen, and Y.-R. Chang, "Simplified reactive power control for single-phase grid-connected photovoltaic inverters," *IEEE Trans. Ind. Electron.*, vol. 61, no. 5, pp. 2286–2296, 2014.
- [40] Y. Yang, F. Blaabjerg, and H. Wang, "Low voltage ride-through of single-phase transformerless photovoltaic inverters," *IEEE Trans. Ind. Appl.*, vol. 50, no. 3, pp. 1942–1952, May/June 2014.
- [41] M. Jang, M. Ciobotaru, and V. G. Agelidis, "A single-phase grid-connected fuel cell system based on a boost-inverter," *IEEE Trans. Power Electron.*, vol. 28, no. 1, pp. 279–288, Jan. 2013.
- [42] M. C. Kısacıkoglu, B. Ozpıneci, and L. M. Tolbert, "EV/PHEV bidirectional charger assessment for V2G reactive power operation," *IEEE Trans. Power Electron.*, vol. 28, no. 12, pp. 5717–5727, Dec. 2013.
- [43] E.ON GmbH, Grid Code-High and Extra High Voltage, 2006.
- [44] H. Wang, M. Liserre, and F. Blaabjerg, "Toward reliable power electronics: Challenges, design tools, and opportunities," *IEEE Ind. Electron. Mag.*, vol. 7, no. 2, pp. 17–26, Jun. 2013.
- [45] H. Huang and P. Mawby, "A lifetime estimation technique for voltage source inverters," *IEEE Trans. Power Electron.*, vol. 28, no. 8, pp. 4113–4119, Aug. 2013.
- [46] Y. Xue *et al.*, "Towards next generation photovoltaic inverters," in *Proc. ECCE*, Sep. 17–22, 2011, pp. 2467–2474.
- [47] Y. Yang, H. Wang, F. Blaabjerg, and K. Ma, "Mission profile based multi-disciplinary analysis of power modules in single-phase transformerless photovoltaic inverters," in *Proc. EPE ECCE Eur.*, Sep. 2–6, 2013, pp. 1–10.
- [48] R. Bayerer, T. Herrmann, T. Licht, J. Lutz, and M. Feller, "Model for power cycling lifetime of IGBT modules—Various factors influencing lifetime," in *Proc. CIPS*, Mar. 2008, pp. 1–6.
- [49] C. Busca *et al.*, "An overview of the reliability prediction related aspects of high power IGBTs in wind power applications," *Microelectron. Rel.*, vol. 51, no. 9–11, pp. 1903–1907, Sep.–Nov. 2011.
- [50] A. T. Bryant, P. A. Mawby, P. R. Palmer, E. Santi, and J. L. Hudgins, "Exploration of power device reliability using compact device models and fast electrothermal simulation," *IEEE Trans. Ind. Appl.*, vol. 44, no. 3, pp. 894–903, May/June 2008.
- [51] Plexim GmbH, PLECS User Manual Version 3.4, Jun. 14, 2013. [Online]. Available: <http://www.plexim.com/>
- [52] A. Wintrich, U. Nicolai, W. Tursky, and T. Reimann, *Application Manual Power Semiconductors*. Nuremberg, Germany: SEMIKRON International GmbH, 2011.
- [53] Y. Avenas, L. Dupont, and Z. Khatir, "Temperature measurement of power semiconductor devices by thermo-sensitive electrical parameters—A review," *IEEE Trans. Power Electron.*, vol. 27, no. 6, pp. 3081–3092, Jun. 2012.



**Yongheng Yang** (S'12–M'15) received the B.Eng. degree in electrical engineering and automation from Northwestern Polytechnical University, Xi'an, China, in 2009 and the Ph.D. degree in electrical engineering from Aalborg University, Aalborg, Denmark, in 2014. During 2009–2011, he was working toward the master–doctoral degree in the School of Electrical Engineering, Southeast University, Nanjing, China, where he was involved in the modeling and control of single-phase grid-connected photovoltaic (PV) systems. From March to May 2013,

he was a Visiting Scholar in the Department of Electrical and Computer Engineering, Texas A&M University, College Station, TX, USA.

He is currently with the Department of Energy Technology at Aalborg University as a Postdoctoral Researcher. His research interest is mainly focused on the control of power electronics for renewable energy systems, particularly for single-phase PV systems, grid integration, reliability in power electronics, and harmonics in adjustable-speed drives and grid-connected converters.



**Huai Wang** (S'07–M'12) received the B.Eng. degree in electrical and electronic engineering from the Huazhong University of Science and Technology, Wuhan, China, in 2007 and the Ph.D. degree in electronic engineering from the City University of Hong Kong, Kowloon, Hong Kong, in 2012.

He has been with Aalborg University, Aalborg, Denmark, since 2012, where he is currently an Assistant Professor in the Department of Energy Technology. He was a Visiting Scientist with the ETH Zurich, Zurich, Switzerland, from August to September 2014 and with the Massachusetts Institute of Technology, Cambridge, MA, USA, from September to November 2013. He was with the ABB Corporate Research Center, Baden, Switzerland, in 2009. He has contributed to over 20 journal papers and filed four patents. His current research interests include the reliability of dc-link and ac filter capacitors, reliability of power electronic systems, high-voltage dc–dc power converters, time-domain control of converters, and passive components reduction technologies.

Dr. Wang is a recipient of six paper awards and project awards from industry, the IEEE, and the Hong Kong Institution of Engineers. He serves as the Guest Associate Editor of the IEEE TRANSACTIONS ON POWER ELECTRONICS Special Issue on Robust Design and Reliability in Power Electronics and the Session Chair of various conferences in power electronics.



**Frede Blaabjerg** (F'03) received the Ph.D. degree from Aalborg University, Aalborg, Denmark, in 1992.

He was with ABB Scandia, Randers, Denmark, from 1987 to 1988. He is currently with Aalborg University, where he became an Assistant Professor in 1992, an Associate Professor in 1996, and a Full Professor of power electronics and drives in 1998. His current research interests include power electronics and applications such as in wind turbines, PV systems, reliability, harmonics, and adjustable-speed drives.

Prof. Blaabjerg has been the recipient of 15 IEEE Prize Paper Awards, the IEEE Power Electronics Society Distinguished Service Award in 2009, the EPE-PEMC Council Award in 2010, the IEEE William E. Newell Power Electronics Award 2014, and the Villum Kann Rasmussen Research Award 2014. He was the Editor-in-Chief of the IEEE TRANSACTIONS ON POWER ELECTRONICS from 2006 to 2012. He was a Distinguished Lecturer of the IEEE Power Electronics Society from 2005 to 2007 and of the IEEE Industry Applications Society from 2010 to 2011.